

Charge transfer and association of Li⁺ colliding with Na from very low to intermediate energiesT. C. Li,¹ Y. Z. Qu,^{1,*} Y. Wu,² L. Liu,² J. G. Wang,² H.-P. Liebermann,³ and R. J. Buenker³¹*College of Material Sciences and Optoelectronic Technology, University of Chinese Academy of Sciences, PO Box 4588, Beijing 100049, China*²*Data Center for High Energy Density Physics, Institute of Applied Physics and Computational Mathematics, PO Box 8009, Beijing 100088, China*³*Fachbereich C-Mathematik und Naturwissenschaften, Bergische Universität Wuppertal, D-42097 Wuppertal, Germany*

(Received 4 November 2014; published 7 May 2015)

The nonradiative charge-transfer processes of Li⁺ + Na(3s) collisions have been investigated by using the fully quantum-mechanical molecular-orbital close-coupling method and the two-center atomic-orbital close-coupling method for the energy range of 10⁻⁴–2 keV/u and 0.2–10 keV/u, respectively. The radiative charge-transfer, radiative decay, and radiative-association processes have been studied by employing the fully quantum, optical-potential, and semiclassical methods for the energy range of 2 × 10⁻¹⁰–110 eV/u. The nonradiative charge-transfer processes dominate the collisions for energies above 0.2 eV/u while radiative decay processes dominate in the lower-energy region. Especially, we found that the radiative-association process is more important than the radiative charge-transfer process when $E < 2 \times 10^{-2}$ eV/u. The rate coefficients of nonradiative and radiative processes are also given for the temperature range of 3 × 10⁴ – 2 × 10⁹ K and 10⁻⁶ – 10³ K, respectively.

DOI: [10.1103/PhysRevA.91.052702](https://doi.org/10.1103/PhysRevA.91.052702)

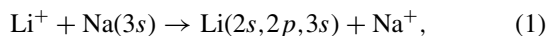
PACS number(s): 34.70.+e, 34.20.Cf, 34.20.Gj

I. INTRODUCTION

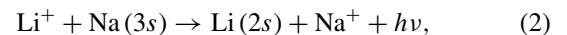
Collisions at cold and ultracold temperatures have been given an important strategic position in the intersectional field of many meaningful research topics in chemical, atomic, molecular, and optical physics, and even in condensed-matter physics [1]. Alkali-metal ion-atom collision systems as main research objects in these areas have recently received considerable attention [2–7]. The charge-transfer and association processes during the collisions are very important for the investigation of charge transport and cold plasmas, because they significantly influence the populations of alkali-metal ions or atoms and their characteristic emission spectra. These spectra are very useful in diagnosing the density of cold laboratory plasmas.

The experimental measurement of electron capture cross sections by Daley and Perel [8] was a stimulating study of the NaLi⁺ system, which presents a standard quasi-one-electron object to investigate the mechanisms of nonresonant charge-transfer processes. Since then, a number of theoretical studies have been performed [9–22]. However, most of them deal with the direct charge-transfer process, and the Li⁺-Na collision system is only studied at the level of total and differential cross sections, whereas investigations of radiative decay processes in the extremely-low-energy (cold) regime are sparse and the information for state-resolved charge-transfer cross sections for the Li⁺-Na collision system is quite rare.

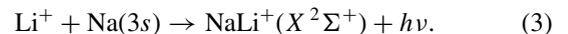
In the present work, we revisit the Li⁺-Na collision system to study both the nonradiative and radiative processes in the energy region from 10⁻¹³ to 10 keV/u. Several reactions are included in our investigation, namely, the nonradiative charge-transfer process,



radiative charge-transfer process,



and radiative-association process,



The nonradiative charge-transfer cross sections are calculated by using the fully quantum-mechanical molecular-orbital close-coupling (QMOCC) and the two-center atomic-orbital close-coupling (TC-AOCC) method in the energy range of 10⁻⁴–2 and 0.2–10 keV/u, respectively. The radiative-decay cross sections are calculated by using the optical-potential and semiclassical methods, respectively, for the energy range of 2 × 10⁻¹⁰ to 110 eV/u. The radiative charge-transfer cross sections are calculated by using the fully quantum method for the energy range of 2 × 10⁻¹⁰–4 × 10⁻⁴ eV/u. The radiative-association cross sections are obtained by taking differences between radiative-decay and radiative charge-transfer cross sections and by using the fully quantum-mechanical approach for the energy range of 2 × 10⁻¹⁰–4 × 10⁻⁴ eV/u and 2 × 10⁻⁵–2 × 10⁻² eV/u, respectively. The molecular structure data (potential curves, radial and rotational couplings, and dipole transition matrix elements) required in the scattering calculations have been calculated using the *ab initio* multireference single- and double-excitation configuration interaction (MRD-CI) method [23,24]. In many application fields, such as astrophysics, the rate coefficients are needed, so we also present the rate coefficients including both radiative and nonradiative processes in this paper.

The present article is organized as follows. In Sec. II we describe the molecular potential and coupling data. In Secs. III and IV we briefly outline the theoretical methods, the results, and discussions of the scattering calculations. A brief summary is given in Sec. V. Atomic units will be used in the remaining part of this article, unless explicitly indicated otherwise.

*yzqu@ucas.ac.cn

TABLE I. Asymptotic separated-atom energies of NaLi⁺.

Molecular state	Asymptotic atomic states	Energy (eV)		
		This work	Experiment [27]	Error
1 ² Σ ⁺	Na ⁺ + Li(2s)	0.252620	0.252638	-1.85[-5] ^a
2 ² Σ ⁺	Na(3s) + Li ⁺	0	0	0
3 ² Σ ⁺	Na ⁺ + Li(2pσ)	-1.546527	-1.595208	4.87[-2]
1 ² Π	Na ⁺ + Li(2pπ)	-1.545511	-1.595208	4.97[-2]
4 ² Σ ⁺	Na(3pσ) + Li ⁺	-2.107886	-2.103718	-4.17[-3]
2 ² Π	Na(3pπ) + Li ⁺	-2.107341	-2.103718	-3.62[-3]
5 ² Σ ⁺	Na ⁺ + Li(3s)	-3.059119	-3.120490	6.14[-2]
6 ² Σ ⁺	Na(4s) + Li ⁺	-3.139746	-3.191351	5.16[-2]

^aNumbers in parentheses are powers, i.e., $A[B] = A \times 10^B$.

II. ELECTRONIC STRUCTURE CALCULATIONS

In the present study, *ab initio* multireference configuration interaction calculations are carried out for adiabatic potential energies of six ²Σ⁺ electronic states in $A_1(C_{2v})$ symmetry and two ²Π electronic states in B_1 symmetry of the NaLi⁺ molecule using the MRD-CI package [23,24]. For lithium, the cc-pVQZ correlation-consistent, polarization valence, quadruple-zeta Gaussian basis set [25] (12s, 6p, 3d)/[5s, 4p, 3d] is used. In addition to the above basis set, (3s3p3d) diffuse functions are added. For sodium atom, an effective core potential (ECP) [26] is employed to describe the two inner-shell electrons, and the remaining inner-shell (2s and 2p) and valence electrons (3s) are considered explicitly in the *ab initio* SCF and CI calculations. The ECP-adapted (6s4p) Gaussian basis set [26] without contraction is employed for the 2s, 2p, and 3s subshells. A diffuse (1s3p3d2f) basis is employed for describing its Rydberg states. A threshold of 1.36×10^{-6} eV (5×10^{-8} hartrees) is used to select the configuration wave functions [23] of which the electronic wave functions are composed. As shown in Table I, the errors in our calculated energies for the considered electronic states with respect to the experimental atomic energies [27] are within 0.0614 eV (491 cm⁻¹) in the asymptotic region. This accuracy level should be adequate for the present scattering calculations [28]. The obtained electronic wave functions are then employed to calculate radial and rotational couplings by using finite differentiation and analytical approaches, respectively [29].

In present QMOCC calculations, allowance for the translation effects was made by introducing appropriate reaction coordinates [30,31], in which the radial and rotational coupling matrix elements between the states ψ_K and ψ_L ($A_{KL}^r = \langle \psi_K | \frac{\partial}{\partial R} | \psi_L \rangle$ and $A_{KL}^\theta = \langle \psi_K | iL_y | \psi_L \rangle$) are transformed into formulas (4) and (5) [32] respectively, where ε_K and ε_L are the electronic energies of states ψ_K and ψ_L , and z^2 and zx are the components of the quadrupole moment tensor. The modification is similar in form to that resulting from the application of the common electron translation factor (ETF) method [33]:

$$\langle \psi_K | \partial / \partial R - (\varepsilon_K - \varepsilon_L) z^2 / 2R | \psi_L \rangle, \quad (4)$$

$$\langle \psi_K | iL_y + (\varepsilon_K - \varepsilon_L) zx | \psi_L \rangle. \quad (5)$$

The calculated adiabatic potentials for the considered six ²Σ⁺ and two ²Π molecular states of NaLi⁺ are shown in Fig. 1 for this internuclear distance $R = 1.0$ – 30.0 a.u. The ²Σ⁺ state represents the initial channel for this collision system. The energy gap between the two lowest states is only about 0.25 eV, which is much smaller than those between ²Σ⁺ and other higher states. Avoided crossings can be observed around 4.0 a.u. between 5²Σ⁺ and 6²Σ⁺ states and at about 7.5 a.u. between 4²Σ⁺ and 5²Σ⁺ states. When R is smaller than 10.0 a.u., the potential curves of the 1²Π state and the ²Σ⁺ state tend to approach each other and become degenerate around $R = 6.0$ a.u., where the rotational coupling between these two states will become important to some extent.

Figures 2 and 3 display some important radial and rotational coupling matrix elements for the NaLi⁺ system with the ETF effects included. Obviously, the positions of the peaks in radial coupling matrix elements are consistent with the corresponding avoided crossings of the adiabatic potential curves observed in Fig. 1. The primary gateway to the

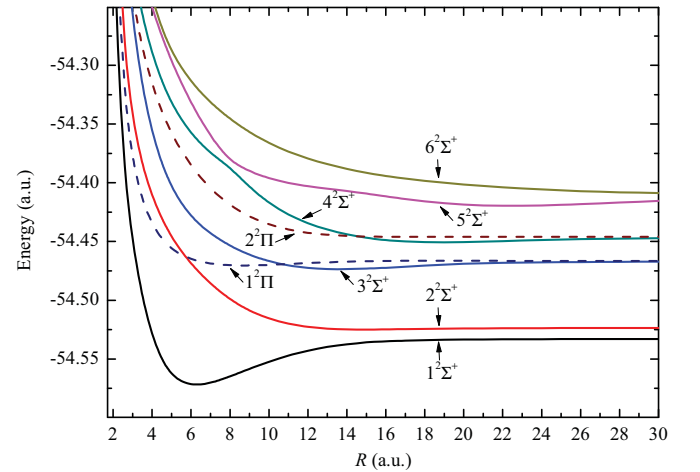


FIG. 1. (Color online) Adiabatic potential curves for NaLi⁺ as a function of internuclear distance R . Solid lines denote the ²Σ⁺ states; dashed lines denote the ²Π states. The 1²Σ⁺, 2²Σ⁺, 3²Σ⁺, 4²Σ⁺, 5²Σ⁺, 6²Σ⁺, 1²Π, and 2²Π states correspond to Na⁺ + Li(2s), Na(3s) + Li⁺, Na⁺ + Li(2pσ), Na(3pσ) + Li⁺, Na⁺ + Li(3s), Na(4s) + Li⁺, Na⁺ + Li(2pπ), and Na(3pπ) + Li⁺ channels in the asymptotic region, respectively.

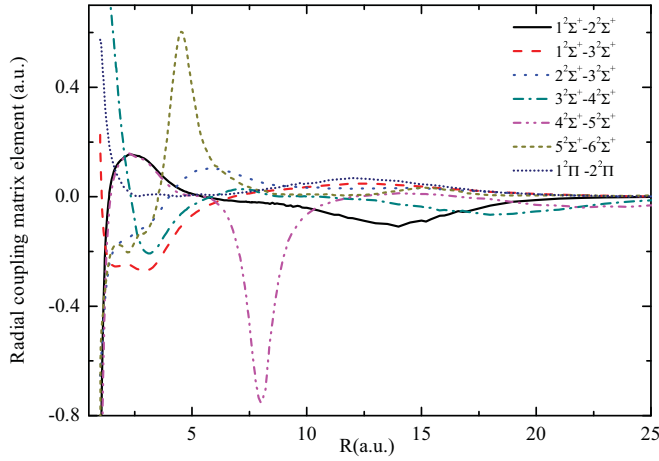


FIG. 2. (Color online) Major radial coupling matrix elements for NaLi⁺.

charge exchange will be the $1^2\Sigma^+ - 2^2\Sigma^+$ and $2^2\Sigma^+ - 1^2\Pi$ couplings as due to the close encounters in the associated potential curves. The importance of the $1^2\Sigma^+ - 2^2\Sigma^+$ and $2^2\Sigma^+ - 1^2\Pi$ transitions has also been observed by the previous work of Melius and Goddard [12,15]. In Fig. 4, the dipole transition moment between the $1^2\Sigma^+$ and $2^2\Sigma^+$ states is distributed in the range of internuclear distances between ~ 1.0 and 30.0 a.u. and a broad peak can be observed around $R = 12.5$ a.u. which corresponds to the position of the avoided crossing between these two states. The dipole transition moment is responsible for the radiative-decay processes in this collision system.

III. THEORIES IN SCATTERING CALCULATIONS

Usually, for the nonradiative charge-transfer process, when the collisional energy E is below several keV/u, the QMOCC method can be applied [31,34], and when E is larger than several hundreds of eV/u, the AOCC method can be used, in which the nuclear motion is treated semiclassically [35].

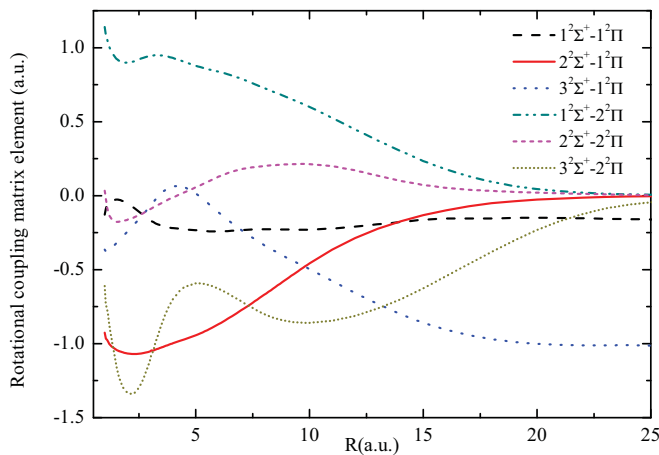


FIG. 3. (Color online) Major rotational coupling matrix elements for NaLi⁺.

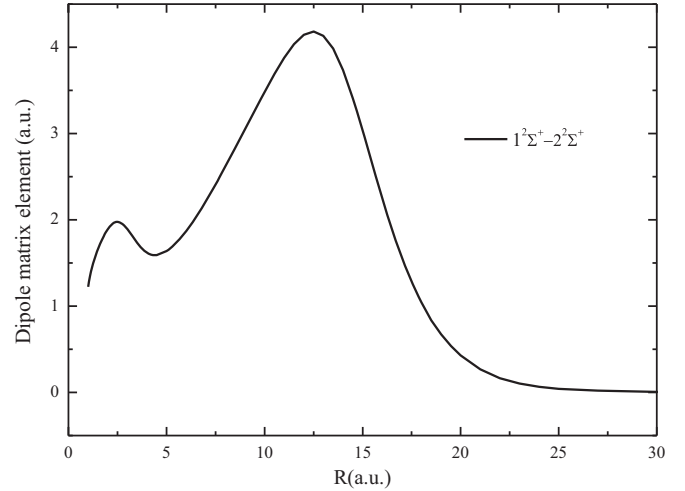


FIG. 4. Dipole matrix element between $1^2\Sigma^+$ and $2^2\Sigma^+$ for NaLi⁺.

A. QMOCC method for nonradiative charge transfer

The QMOCC method to describe nonradiative charge transfer in ion-atom collisions is described in detail in the literature [31,34], and will be only briefly outlined here. In the QMOCC method, the collision system composed of ion and an atom or molecule is treated as a quasimolecule, the internuclear distance of which varies with the collision time. Besides, a close-coupled quantum-mechanical method is employed for the motion of the system. It involves solution of a coupled set of second-order differential equations using the log-derivative method of Johnson [36]. In the adiabatic representation, transitions between channels are driven by radial and rotational (A^r and A^θ) coupling elements of the vector potential $A(\vec{R})$, where \vec{R} is the internuclear distance vector. Since the adiabatic description contains first- and second-order derivatives, it is numerically convenient to make a unitary transformation [34,37] to a diabatic representation,

$$U(R) = W(R)[V(R) - P(R)], \quad (6)$$

where $U(R)$ is the diabatic potential matrix, $V(R)$ is the diagonal adiabatic potential, $W(R)$ is a unitary transformation matrix that obeys the equation

$$dW(R)/dR + A^r(R)W(R) = 0, \quad (7)$$

and $P(R)$ is the rotational coupling matrix of the vector potential $A(\vec{R})$ whose elements are given by [31,38]

$$P_{ij} = \mp \frac{1}{\mu R^2} [(J \mp \Lambda_i)(J \pm \Lambda_i + 1)]^{1/2} A_{ij}^\theta \delta(\Lambda_i, \Lambda_j \pm 1). \quad (8)$$

The coupled set of second-order differential equations is solved by employing the diabatic potential and couplings. The charge-capture cross section from initial channel i to the final channel j is given by

$$\sigma_{(i \rightarrow j)} = \frac{\pi}{k_i^2} \sum_J (2J + 1) |S_J|_{i,j}^2; \quad (9)$$

here k_i denotes the initial momentum, J is the total angular momentum, and S the scattering matrix,

$$S_J = [I + iK_J]^{-1}[I - iK_J], \quad (10)$$

where I is the identity matrix, and the K matrix is obtained from the scattering amplitude after a partial-wave decomposition [39].

B. TC-AOCC method for nonradiative charge transfer

The AOCC method is a semiclassical theoretical method, in which the motion of the nucleus meets the classical law. The motion of electrons is obtained by solving the Schrödinger equation of the collision system. The TC-AOCC equations are obtained by expanding the total electron wave function Ψ in terms of atomic orbitals of the two centers (ϕ_i^A, ϕ_j^B) multiplied by plane-wave electron translational factors (ETFs) [35],

$$\Psi(\vec{r}, t) = \sum_i a_i(t) \phi_i^A(\vec{r}, t) + \sum_j b_j(t) \phi_j^B(\vec{r}, t), \quad (11)$$

and its insertion in the time-dependent Schrödinger equation (TDSE) $(H - i\frac{\partial}{\partial t})\Psi(\vec{r}, t) = 0$. Here, $H = -\frac{1}{2}\nabla_r^2 + V_A(r_A) + V_B(r_B)$ and $V_{A,B}(r_{A,B})$ are electron interactions with the projectile (Li^+) and target (Na^+) cores, respectively. The straight-line approximation is adopted for the relative nuclear motion in this collision system. For the Li^+ and Na^+ ions, the frozen core approximation is employed. The interaction of the active electron with the ionic cores can be expressed by model potentials as [40] (for Li^+) and as [4] (for Na^+),

$$V_{\text{Li}^+}(r) = -\frac{1}{r} - \frac{1}{r}(2 + 3.310r)e^{-3.310r}, \quad (12)$$

$$V_{\text{Na}^+}(r) = -\frac{1}{r} - \frac{1}{r}(10 + 17.9635r)e^{-3.5927r}. \quad (13)$$

The resulting first-order coupled equations for the amplitude $a_i(t)$ and $b_j(t)$ are

$$i(\dot{A} + S\dot{B}) = HA + KB, \quad (14a)$$

$$i(\dot{B} + S^\dagger\dot{A}) = \bar{K}A + \bar{H}B, \quad (14b)$$

where A and B are the vectors of the amplitudes $a_i(t)$ ($i = 1, 2, \dots, N_A$) and $b_j(t)$ ($j = 1, 2, \dots, N_B$), respectively. S is the overlap matrix (S^\dagger is its transposed form). H and \bar{H} are direct coupling matrices, and K and \bar{K} are the electron exchange matrices. The cross section for $1 \rightarrow j$ electron capture transitions is calculated as

$$\sigma_{cx,j} = 2\pi \int_0^\infty |b_j(+\infty)|^2 b db, \quad (15)$$

where b is the impact parameter.

The sum of $\sigma_{cx,j}$ over j gives the corresponding total charge-transfer cross section. The expansion basis used in present TC-AOCC calculations includes all states centered on Li^+ having principal quantum number $n \leq 5$ and all states on Na having principal quantum number $n \leq 5$, without the $4f$, $5f$, and $5g$ orbitals. To check the convergence, we have calculated the total cross section and the state-selective cross section with the bound states up to $n = 5$ and 6 for Li^+ . For the collision energies from 0.3 to 5.0 keV/u, the relative discrepancies between the results of these two calculations for

the total cross sections and the state-selective cross sections for electron capture to $\text{Li}(2s)$ and $\text{Li}(2p)$ are within 1%, 1%, and 3%, respectively. To check the influence of the pseudocontinuum states, we also calculated the total cross section and the state-selective cross section of each state with the bound states up to $n = 5$ and the pseudocontinuum states $6s^*$, $6p_{|m|}^*$, $6d_{|m|}^*$, $6f_{|m|}^*$, $6g_{|m|}^*$ for Li^+ . For the collision energies E from 0.3 to 5.0 keV/u, the relative discrepancies between the results with and without the pseudocontinuum states of the total cross sections and the state-selective cross sections for electron capture to $\text{Li}(2s)$ and $\text{Li}(2p)$ are within 5%, 15%, and 7%, respectively. So, the $6s^*$, $6p_{|m|}^*$, $6d_{|m|}^*$, $6f_{|m|}^*$, $6g_{|m|}^*$ pseudostates which lie in the continuum of the lithium atom are also included in the basis.

For systems that do not have strong radial couplings, radiative processes such as radiative charge-transfer and radiative association play important roles at the very-low-energy region. The quantum-mechanical method and the semiclassical method were used for calculations of the radiative processes for the energy range of 2×10^{-10} – 110 eV/u.

C. Fully quantum method for radiative charge transfer

In the present work, the fully quantum-mechanical method [41–43] is used to investigate the radiative charge-transfer process. The radiative charge-transfer cross section can be given by

$$\sigma = \int_{\omega_{\min}}^{\omega_{\max}} \frac{d\sigma}{d\omega} d\omega, \quad (16)$$

with

$$\begin{aligned} \frac{d\sigma}{d\omega} = & \frac{8}{3} \left(\frac{\pi}{k_A} \right)^2 \frac{\omega^3}{c^3} \sum_J [JM_{J,J-1}^2(k_A, k_X) \\ & + (J+1)M_{J,J+1}^2(k_A, k_X)], \end{aligned} \quad (17)$$

where ω is the angular frequency of the emitted photon and c is the speed of light. The subscripts A and X denote the upper and the lower states, respectively, and

$$M_{J,J'}(k_A, k_X) = \int_0^\infty dR f_J^A(k_A R) D(R) f_{J'}^X(k_X R), \quad (18)$$

where $D(R)$ is the transition dipole moment connecting the two electronic states, k_A and k_X are the entrance and exit momenta,

$$k_A = \sqrt{2\mu[E - V_A(\infty)]}, \quad (19a)$$

$$k_X = \sqrt{2\mu[E - V_X(\infty)] - \hbar\omega}, \quad (19b)$$

with E the relative collision energy in the center-of-mass frame, and V_A and V_X are the adiabatic potential energies of the entrance and exit channels, respectively. The partial wave $f_J^i(k_i R)$ ($i = A, X$) is the regular solution of the homogeneous radial equation

$$\begin{cases} \frac{d^2}{dR^2} - \frac{J(J+1)}{R^2} - 2\mu[V_i(R) - V_i(\infty)] + k_i^2 \\ f_J^i(k_i R) = 0, \end{cases} \quad (20)$$

and normalized asymptotically according to

$$f_j^i(k_i R) = \sqrt{\frac{2\mu}{\pi k_i}} \sin\left(k_i R - \frac{J\pi}{2} + \delta_j^i\right), \quad (21)$$

with δ_j^i , ($i = A, X$) the phase shifts.

D. Optical-potential and semiclassical methods for radiative decay

The optical-potential approach [41,42,44] is adopted to obtain the total cross sections for radiative decay, including both the radiative charge transfer and the radiative association. During the ion-atom collisions, the transition probability is represented by the imaginary part of a complex optical potential. The scattering wave $F_A(\vec{R})$, where R is the internuclear distance and the subscript A denotes the initial upper molecular state ($A^2\Sigma^+$), is obtained by solving the Schrödinger equation,

$$\left[-\frac{1}{2\mu}\nabla_{\vec{R}}^2 + V_A(R) - E\right]F_A(\vec{R}) = \frac{i}{2}A(R)F_A(\vec{R}). \quad (22)$$

Here E is the collision energy of the entrance channel, μ is the reduced mass, and $A(R)$ is the transition probability for the radiative transition given by

$$A(R) = \frac{4}{3}D^2(R)\frac{|V_A(R) - V_X(R)|^3}{c^3}, \quad (23)$$

where $V_A(R)$ and $V_X(R)$ are the adiabatic potential energies for the upper $A^2\Sigma^+$ and the lower $X^2\Sigma^+$ states, respectively. $D(R)$ is the transition dipole matrix element between the $A^2\Sigma^+$ and $X^2\Sigma^+$ states.

The collision-induced radiative decay cross sections can be written as

$$\sigma(E) = \frac{\pi}{k_A^2} \sum_J (2J+1)[1 - \exp(-4\eta_J)], \quad (24)$$

where η_J is the imaginary part of the phase shift for the J th partial wave of the radial Schrödinger equation which is given in the distorted-wave approximation by

$$\eta_J = \frac{\pi}{2} \int_0^\infty dR |f_J^A(k_A R)|^2 A(R). \quad (25)$$

The optical-potential method provides an adequate description of the radiative decay process only at low (below ~ 0.1 eV) collision energies. In order to extend our radiative decay calculations to higher energies, replacing the summation in Eq. (24) and applying the Jeffreys-Wentzel-Kramers-Brillouin (JWKB) approximation, one obtains an expression for the semiclassical cross section,

$$\sigma(E) = 2\pi \sqrt{\frac{2\mu}{E}} \int pdp \int_{R_A^{\text{ctp}}}^\infty dR \frac{A(R)}{\sqrt{1 - V_A(R)/E - p^2/R^2}}, \quad (26)$$

where p is the impact parameter and R_A^{ctp} is the classical turning point in the incoming channel [41,45]. For large energies ($E \gg V_A$), the double integral is nearly energy independent, and therefore $\sigma(E)$ varies as $1/E^{1/2}$ [42,44]. By subtracting the radiative charge-transfer part from the

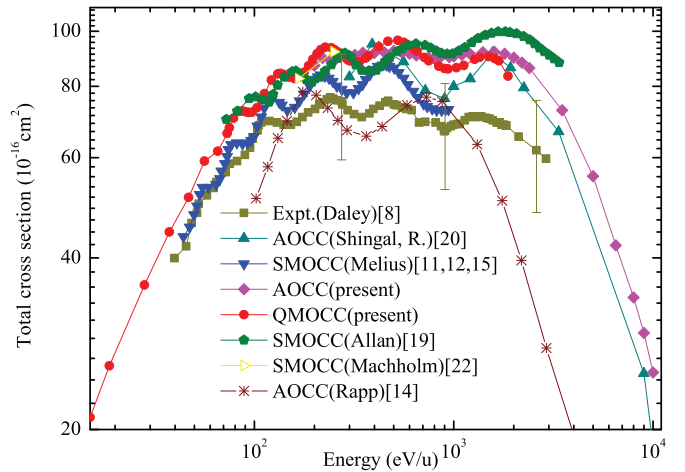


FIG. 5. (Color online) The total nonradiative charge-transfer cross sections of the present calculation and other results for Na(3s) + Li⁺ collision. Theoretical results: present QMOCC calculation (solid line with filled circles), present AOCC calculation (solid line with filled diamond), Melius *et al.* [11,12,15] (solid line with filled downward triangle), Allan *et al.* [19] (solid line with filled pentagon), Machholm *et al.* [22] (solid line with filled right triangle), Shingal *et al.* [20] (solid line with filled upward triangle), Rapp *et al.* [14] (solid line with star).

total radiative-decay cross sections, one obtains the radiative-association cross sections.

IV. RESULTS AND DISCUSSION

A. Nonradiative charge transfer

The total nonradiative charge-transfer cross sections in collisions of Li⁺ with ground state atomic Na are investigated by using the QMOCC method in the energy range 10^{-3} –1.8 keV/u, and the TC-AOCC method is also used for comparison and to extend the calculation to the higher-energy region (0.2–10⁴ keV/u), which are displayed in Fig. 5, along with the experimental results of Daley and Perel [8] and other theoretical works [11,12,15,19,20,22]. The present QMOCC and AOCC results are in good agreement in the overlapping energy range around 1 keV/u, where both of the two theoretical methods are reliable. Our QMOCC results agree well with the SMOCC (semiclassical molecular-orbital close-coupling) results of Machholm [22] and Allan [19] in the energy region below 1 keV/u. Our AOCC results agree well with those of Shingal *et al.* [20] only for energy around 420 and 1560 eV/u, but obvious discrepancy can be found for other energies; the probable reason is that their results are not fully converged, as they themselves claimed in Ref. [20]. The calculation of total cross section carried out by Melius and Goddard [11,12,15] was considered to be the best theoretical prediction [17], since they find excellent agreement with the experimental results of Daley and Perel [8]. However, our present calculated total charge-transfer cross sections are about 20% higher than those of Melius and Goddard. A possible reason is because of the difference of the potential curves; e.g., their error of energy in the asymptotic region is about 0.1 eV [14], which is larger than ours compared to the experimental data from NIST [27]

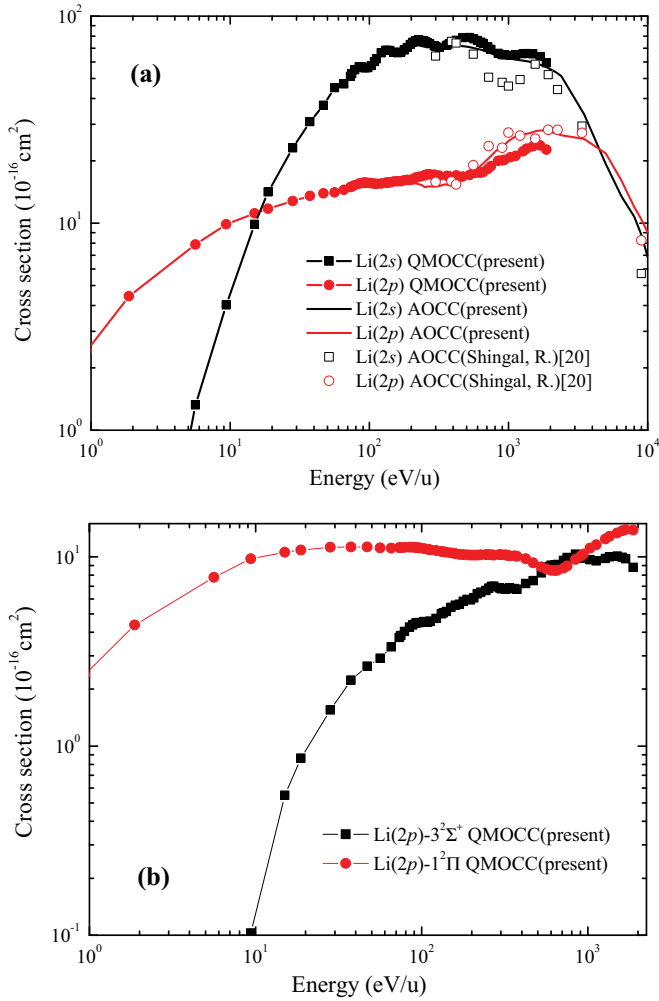


FIG. 6. (Color online) (a) State-selective nonradiative charge-transfer cross sections for the $\text{Na}(3s) + \text{Li}^+$ collision. Shown are present QMOCC results (solid line with symbols); present AOCC results (solid lines); AOCC results of Shingal *et al.* (open symbols); (b) state-selective cross sections for electron capture to the $3^2\Sigma^+$ and $1^2\Pi$ states of NaLi^+ .

(see Table I). Also, from Fig. 5, there is good agreement in the positions and amplitude of oscillatory structures between the experimental cross sections [8] and ours. However, for the value of total cross section, our QMOCC and AOCC results are higher than that of experiment [8]. For energy around 274 eV/u, our results are near the upper limit of the experimental error bar. For energy around 905 and 2600 eV/u, they exceed the upper limit. In view of the fact that the experiment of Daley and Perel [8] is rather old, the difference in the amplitude of total cross section between their measurement and our calculation may be due to the calibration of the experiment, so new experimental measurements are needed.

To obtain more detailed information, the state-selective cross sections are shown in Fig. 6. The results of electron capture to $\text{Li}(2s)$ and $\text{Li}(2p)$ states are presented in Fig. 6(a), which agree with Shingal's AOCC calculations [20] in the energy region of 200–2000 eV/u for $\text{Li}(2p)$ states, and also around 420 and 1560 eV/u for $\text{Li}(2s)$. However, in other energy regions, obvious discrepancy exists. As in Fig. 5, the

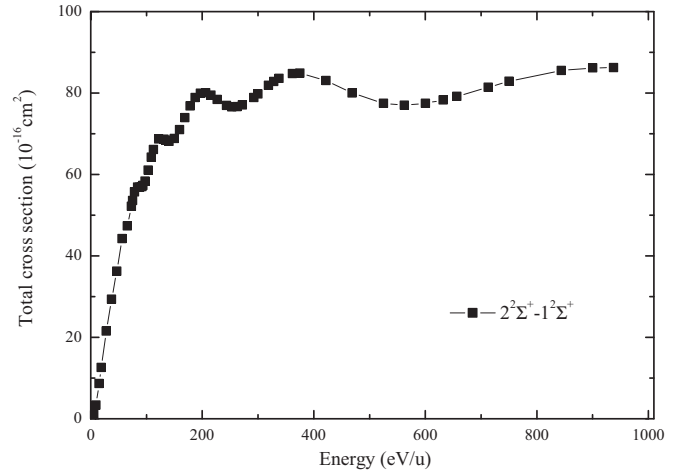


FIG. 7. The total nonradiative charge-transfer cross sections using two-state ($1^2\Sigma^+$, $2^2\Sigma^+$) approximation for collisions of $\text{Na}(3s) + \text{Li}^+$.

probable reason is that their calculation is not converged [20]. The charge transfer to the $\text{Li}(2s)$ state dominates the magnitude and detailed structure of the total cross sections because of the small energy gap between the $2^2\Sigma^+$ and $1^2\Sigma^+$ potential curve (see Fig. 1). The electron capture to the $\text{Li}(2p)$ state becomes important for energies below 10 eV/u. State-selective cross sections to the $3^2\Sigma^+$ and $1^2\Pi$ channels are presented in Fig. 6(b), which shows the $1^2\Pi$ channel is dominant in the lower-energy region ($E < 1000$ eV/u); above that, the two channels are comparable. This is consistent with the energy potential curves (see Fig. 1) and the magnitude of the relevant couplings (see Figs. 2 and 3). In the higher-energy region ($E > 1000$ eV/u), the electron capture processes are mainly triggered by the radial and rotational couplings at small internuclear distances, where potential curves for the $2^2\Sigma^+$, $3^2\Sigma^+$, and $1^2\Pi$ are very close to each other. The couplings between these states will influence the charge-transfer processes, and the electron population in these three states indicates competition between them. As the energy decreases, the energy gap between the $2^2\Sigma^+$ and $3^2\Sigma^+$ states increases and also there is no strong radial coupling between them. Therefore, the state-selective charge-transfer cross section to $3^2\Sigma^+$ drops rapidly. As collision energies decrease, the potential curves of the $2^2\Sigma^+$ and $1^2\Pi$ states are still close to each other and become degenerate around $R = 6.0$ a.u. As a result, the strong and broad effect coming from the rotational coupling between the $2^2\Sigma^+$ and $1^2\Pi$ states will cause the state-selective cross section to $1^2\Pi$ to become dominant in the lower-energy region. This is the reason why the electron capture to the $\text{Li}(2p)$ state becomes dominant when the energy drops below 10 eV/u [see Fig. 6(a)].

Also from Figs. 5 and 6(a), there exists obvious oscillatory structure in the total and state-selective cross section. To check if this is caused by the interference between final states such as $1^2\Sigma^+$, $3^2\Sigma^+$, and $1^2\Pi$, we carried out a two-state ($1^2\Sigma^+$, $2^2\Sigma^+$) calculation, with only one final state $1^2\Sigma^+$ as shown in Fig. 7, in which the oscillations still exist. This shows that the origin of the oscillatory structure is not simply the interference between the final states. Such oscillatory structure

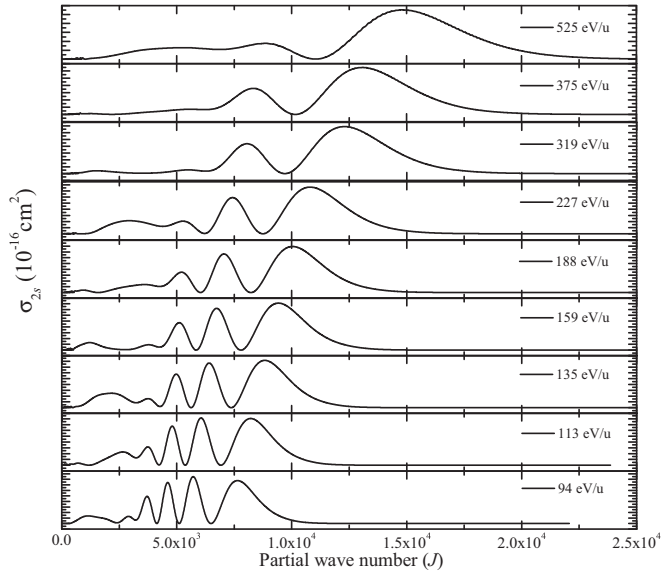


FIG. 8. Partial-wave cross sections of electron capture to the Li(2s) state for collisions of Na(3s) + Li⁺.

may be interpreted as a type of Stueckelberg oscillation, which is due to a nonrandom-phase contribution to the cross sections caused by one or more extrema in the difference between the potentials for the reactant and product states [9,13]. To get more information about these oscillations, we calculated the partial-wave cross sections of electron capture into the Li(2s) state for nine different collision energies from 94 to 525 eV/u, among which 94, 159, and 319 eV/u correspond to three local minima in the charge-transfer cross sections to the Li(2s) state, and 135, 227, and 525 eV/u correspond to three local maxima. The resulting partial-wave cross sections are given in Fig. 8, where the oscillatory structure in the charge-transfer cross sections mainly depends on the partial waves with small numbers which are very sensitive to the collision energy. As the collision energy increases, peaks in the partial-wave cross sections shift toward larger partial-wave numbers. The overall magnitude of the cross sections depends primarily upon partial waves with large numbers. This result is similar to that of Rapp *et al.* [14], since the behaviors of partial-wave cross sections with small or large numbers J in our quantum-mechanical calculations correspond to those with small or large impact parameters in their work. However, only the atomic-orbital expansion is included in their calculation; it cannot adequately account for collisions at small impact parameter [14]. As a result, the detailed structure represented by their calculation disagrees substantially with the experimental data of Daley and Perel [8], as shown in Fig. 5.

B. Radiative decay, radiative charge transfer, and radiative association

For radiative processes of Na + Li⁺, the upper A and the lower X states in Eqs. (17)–(26) correspond to the $2^2\Sigma^+$ and the $1^2\Sigma^+$ states of NaLi⁺, respectively. In this case, one only need consider the radiative processes from the initial channel of the $2^2\Sigma^+$ state to the lower $1^2\Sigma^+$ state, which is dominated by the long-range polarization interaction. In our calculation,

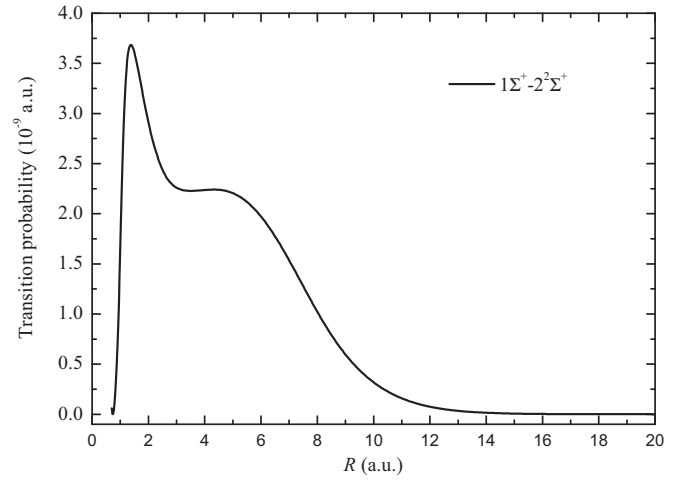


FIG. 9. Transition probability between the $1^2\Sigma^+$ and the $2^2\Sigma^+$ states as a function of internuclear distance.

the values of R_{\max} for matching the boundary conditions are increased from 500 to 2000 a.u. for collision energies varying from 110 to 2×10^{-10} eV/u. Beyond $R = 15$ a.u., the potentials of the $1^2\Sigma^+$ and the $2^2\Sigma^+$ states are described by the long-range form

$$V_L(R) = -\frac{1}{2} \left[\frac{C_4}{R^4} + \frac{C_6}{R^6} + \frac{C_8}{R^8} \right], \quad (27)$$

where C_4 , C_6 , and C_8 are the dipole, quadrupole, and octupole polarizabilities of Li(2s) and Na(3s) atom, respectively [46]. Based on the potential energy obtained, the transition probability $A(R)$ is computed using Eq. (23), as shown in Fig. 9. There are two peaks; one is a sharp peak near $R = 1.4$ a.u. and the other is a broad peak near $R = 5.0$ a.u. The transition probability approaches zero as the internuclear distance increases beyond 15.0 a.u.

As shown in Fig. 10, the radiative-decay (including radiative charge-transfer and radiative association) cross sections are calculated for collision energies from 2×10^{-10} to 3×10^{-2} eV/u by using the optical-potential method; the computational cost increases rapidly for higher collision energies. In order to extend the treatment to higher energies, a semiclassical calculation has been performed using Eq. (26) for collision energies of 2×10^{-6} – 110 eV/u. In the overlapping energy range of 2×10^{-6} – 3×10^{-2} eV/u, except for the resonance behavior, the semiclassical cross sections are in good agreement with the optical-potential results. The resonant structures, appearing in the energy region of 2×10^{-10} – 2×10^{-3} eV/u, are attributed to the presence of quasibound or virtual rotational-vibrational levels in the entrance channel [7,42–44,47–52]. In the semiclassical approach, no quasibound or virtual rotational-vibrational levels exist; thus the semiclassical approximation is believed to be able to give reliable cross sections in the higher-energy region. Apart from the resonant structures, the radiative-decay cross sections increase monotonically as the collision energies decrease. Significantly, our cross sections have an energy dependence of $1/E^{1/2}$, which is consistent with the classical Langevin cross-section formula for a polarization potential. However, when the relative energy increases continuously, the semiclassical cross sections ascend

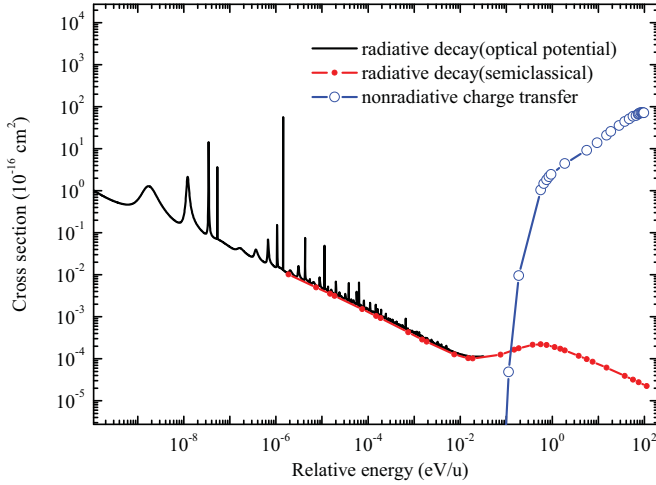


FIG. 10. (Color online) Comparison of the radiative-decay and nonradiative charge-transfer cross sections for $\text{Na}(3s) + \text{Li}^+$ collision. Radiative decay cross sections are obtained by the optical-potential method (solid line) and the semiclassical method (solid line with solid circles), respectively, and nonradiative charge-transfer cross sections (solid line with open circles) are obtained by the QMOCC method.

gradually until reaching a maximum at ~ 0.75 eV/u and then decrease as $1/E^{1/2}$. This behavior can be understood from the potential curves and transition probabilities. For the initial state $2^2\Sigma^+$, the corresponding classical turning point R_a^{ctp} is less than 11.0 a.u. when the relative energy is more than 2×10^{-2} eV/u, as shown in Fig. 1. The transition probability $A(R)$ in Eq. (23), which is displayed in Fig. 9, increases rapidly as R decreases, so that the integral in Eq. (26) increases faster than the factor of $1/E^{1/2}$ as the collision energy increases and the R_a^{ctp} decreases, resulting in an increasing tendency for the cross section. When the relative energy is more than 0.9 eV/u, the classical turning point R_a^{ctp} is less than 3.0 a.u. Thereafter, the variation of $A(R)$ tends to zero and the integral in Eq. (26) does not increase further and $\sigma(E)$ varies as $1/E^{1/2}$. We should also note that the transition probability $A(R)$ increases rapidly once again as R decreases to less than 2.5 a.u., but the cross sections do not show an obvious increasing tendency. This is because, when R is less than 2.5 a.u., the collision energy E in the denominator of the integral term in Eq. (26) dramatically increases and thus the effect caused by the variation of the transition probability $A(R)$ is offset.

In Fig. 10, we also compare the present radiative-decay cross sections with the present nonradiative charge-transfer cross sections calculated by using the QMOCC method. For energies less than 0.1 eV/u, the radiative-decay processes are dominant and the nonradiative charge-transfer processes are negligible, where the electronic transitions are driven through the weak avoided crossing between $1^2\Sigma^+$ and the $2^2\Sigma^+$ states at an internuclear distance of $R = 12.5$ a.u. As the collision energy increases, the nonradiative charge-transfer cross sections increase rapidly. The nonradiative process becomes the dominant charge-transfer mechanism for energies larger than $E > 0.2$ eV/u, where the electronic transitions occur through the rotational coupling between the $2^2\Sigma^+$ and the $1^2\Pi$ states.

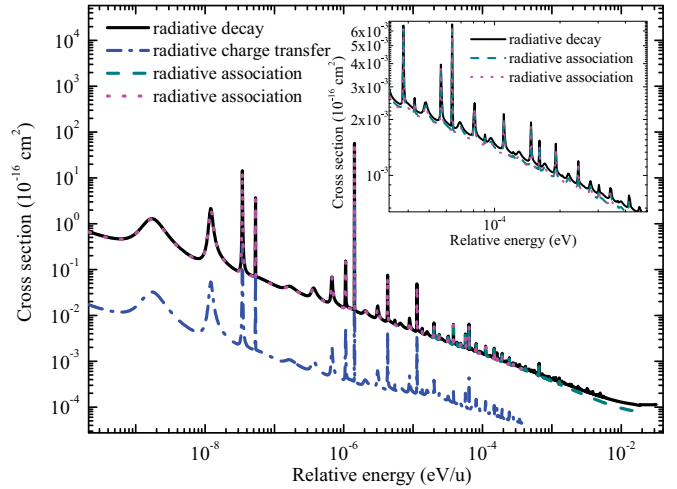


FIG. 11. (Color online) Comparison of the radiative-decay (solid line), radiative charge-transfer (dashed line with dot), and radiative-association cross sections for collisions involving the $2^2\Sigma^+ - 1^2\Sigma^+$ transition in the $\text{Na}(3s) + \text{Li}^+$. Radiative-association cross sections are obtained by the fully quantum-mechanical approach (dashed line) and the subtracting method (dotted line), respectively.

The radiative charge-transfer and radiative-association cross sections are presented along with the radiative-decay cross sections for the energy range of $2 \times 10^{-10} - 2 \times 10^{-2}$ eV/u in Fig. 11. In our present calculations, for the energy region from 2×10^{-10} to 4×10^{-4} eV/u, the radiative charge-transfer cross sections are obtained by using the fully quantum-mechanical method and the radiative-association cross sections are calculated by subtracting the radiative charge-transfer part from the total radiative-decay cross sections. For collision energies from 2×10^{-5} to 2×10^{-2} eV/u, the fully quantum-mechanical approach has been used again to describe the radiative association in the $\text{Na}(3s) + \text{Li}^+$ collisions. The inset illustration shows that the radiative-association cross sections obtained by using the two different methods are in excellent agreement with each other in the overlapping energy range. In Fig. 11, the association process is seen to be more important than the charge transfer: The radiative charge-transfer cross sections are about two orders of magnitude smaller than the radiative-association cross sections. However, as the collision energy increases, the difference between the radiative-association and charge-transfer cross sections decreases. The radiative-association cross sections decrease more rapidly than that of the radiative charge transfer. This is because of the fact that the effective angular momentum numbers increase with collision energy, and this could result in a shallower well of the effective potential $V_J^{\text{eff}}(R) = V(R) + J(J+1)/2\mu R^2$ for the final state of $1^2\Sigma^+$, causing the number of the quasibound vibrational levels to become smaller.

C. Rate coefficients

Rate coefficients are very useful in many application fields, such as astrophysics. The rate coefficients for total and state-selective nonradiative charge-transfer processes of $\text{Na}(3s) + \text{Li}^+$ collisions are calculated by averaging

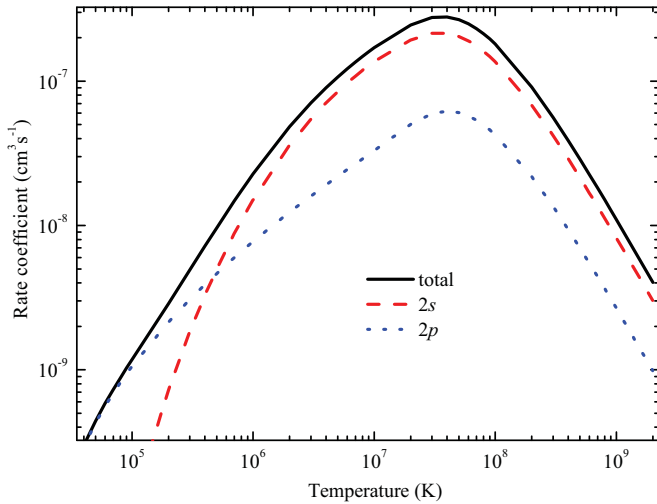


FIG. 12. (Color online) Rate coefficients as a function of temperature for total and state-selective nonradiative charge-transfer processes of Na(3s) + Li⁺ collisions.

the corresponding cross sections for collision energy from 0.001 to 1.8 keV/u over a Maxwellian velocity distribution as a function of temperature T from 3×10^4 to 2×10^9 K, as shown in Fig. 12. They are consistent with total and state-selective cross sections. For $T < 3 \times 10^4$ K, the rate coefficients decrease rapidly and the radiative process will become dominant. The rate coefficients are fitted to the form

$$\alpha(T) = \sum_i a_i \left(\frac{T}{10,000} \right)^{b_i} \exp\left(-\frac{T}{c_i}\right), \quad (28)$$

where α is the rate coefficient in $\text{cm}^3 \text{s}^{-1}$ and T is the temperature in K. For convenience of application, the fitting parameters of rate coefficients for temperatures between 3×10^4 and 2×10^9 K are given in Table II. The fitting coefficients of determination are larger than 0.9996, which indicates that our fit of Eq. (28) is accurate.

The total radiative decay, radiative-association, and radiative charge-transfer rate coefficients are also obtained by averaging the cross sections over a Maxwellian velocity

TABLE II. Fitting parameters of rate coefficients for total and state-selective nonradiative charge-transfer processes. The units of fitting parameters a_i and c_i are $\text{cm}^3 \text{s}^{-1}$ and K, respectively.

Parameters	Value		
	2s	2p	Total
a_1	8.2122[−7] ^a	2.7815[−13]	−7.7871[−7]
a_2	2.5727[−7]	−4.9046[−6]	−9.5556[−4]
a_3	−1.0722[−6]	4.9062[−6]	9.5556[−4]
b_1	−1.2530[−1]	1.5744	6.5474[−2]
b_2	−1.3114[−1]	−5.1020[−1]	−9.1787[−1]
b_3	−1.2170[−1]	−5.1089[−1]	−9.1774[−1]
c_1	8.1222[7]	2.5442[7]	1.8604[7]
c_2	4.8261[8]	4.8056[7]	1.3083[7]
c_3	1.8456[7]	5.1758[8]	1.1136[9]

^aNumbers in parentheses are powers, i.e., $A[B] = A \times 10^B$.

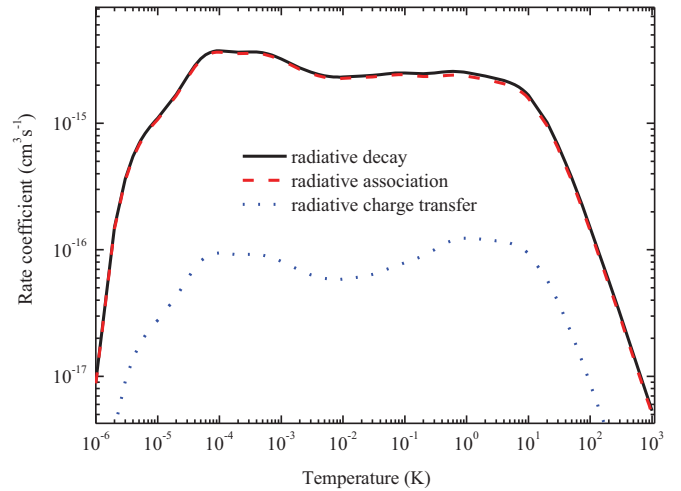


FIG. 13. (Color online) Rate coefficients as a function of temperature for radiative decay, radiative-association, and radiative charge-transfer processes of Na(3s) + Li⁺ collisions.

distribution and then plotting them as a function of temperature from 10^{-6} to 10^3 K, as shown in Fig. 13. It can be seen that, in this range of temperature, the dominant radiative process is radiative association and its rate coefficient is about two orders of magnitude larger than that of radiative charge transfer, which is consistent with the cross-section data (see Fig. 11). Above 10^{-6} K, each curve of the rate coefficient increases rapidly with increasing temperature, and then approaches a constant value between 10^{-4} and 10 K, which is caused by the fact that the cross section behaves as $1/E^{1/2}$ (the Langevin behavior). For $T > 1000$ K, the contribution from nonradiative processes becomes dominant.

Also for convenience of application, the rate coefficients of radiative processes are fitted into the same form as for Eq. (28). The fitting parameters are provided in Table III in the entire

TABLE III. Fitting parameters of rate coefficients for total radiative decay, radiative-association, and radiative charge-transfer processes. The units of fitting parameters a_i and c_i are $\text{cm}^3 \text{s}^{-1}$ and K, respectively.

Parameters	Value		
	Radiative decay	Radiative association	Radiative charge transfer
a_1	1.8383[−15] ^a	1.9290[−13]	1.3554[−16]
a_2	3.5888[−16]	1.7114[−15]	2.2523[−17]
a_3	−1.2267[−12]	2.9669[−15]	−5.1364[−17]
a_4	−3.7277[−17]	−2.8569[−15]	−6.0105[−17]
b_1	−4.0294[−2]	1.1626	1.5289[−3]
b_2	−1.1029[−1]	−4.6141[−3]	−5.0903[−2]
b_3	2.8292[−1]	1.8901[−2]	−2.8502[−2]
b_4	−2.3054[−1]	−1.3399[−2]	−2.4797[−2]
c_1	2.6915[1]	5.3753[1]	2.7170[1]
c_2	1.8443[−3]	1.5103[−3]	1.8553[−3]
c_3	2.2683[−5]	1.8337[1]	3.6281[−1]
c_4	5.0947[−1]	3.2601[−5]	3.3239[−5]

^aNumbers in parentheses are powers, i.e., $A[B] = A \times 10^B$.

temperature range from 10^{-6} to 10^3 K. The fitting coefficients of determination are larger than 0.9971, so our fit of Eq. (28) is also accurate.

V. CONCLUSION

In the present work, we present the charge-transfer cross sections in a very wide energy range. Cross sections have been calculated for the nonradiative charge-transfer processes due to collisions of Li^+ with neutral sodium in the energy range of 10^{-4} – 2 keV/u and 0.2 – 10 keV/u by employing the QMOCC and TC-AOCC methods, respectively. Our QMOCC and AOCC results merge well in the overlapping energy range. Good agreement has been found between the two calculations for both the total and the state-resolved capture cross sections. The rotational couplings play very important roles in the low-energy region. The origin of the oscillatory structure is not simply the interference between the final states. Such oscillatory structure may be interpreted as a type of Stueckelberg oscillation.

The radiative-decay process is investigated by using the optical-potential and semiclassical methods in the collision energy range of 2×10^{-10} – 3×10^{-2} eV/u and 2×10^{-6} – 110 eV/u, respectively, and the two calculations join

together smoothly in the energy range of 2×10^{-6} – 3×10^{-2} eV/u. The radiative charge-transfer cross sections are calculated by using the fully quantum method in the energy range of 2×10^{-10} – 4×10^{-4} eV/u. The radiative-association cross sections are obtained by subtracting the radiative charge-transfer part from the radiative-decay cross sections and by using the fully quantum-mechanical approach, respectively, for the energy range of 2×10^{-10} – 4×10^{-4} eV/u and 2×10^{-5} – 2×10^{-2} eV/u. The radiative processes exceed the nonradiative process as $E < 0.11$ eV/u. In particular, we found that the radiative-association process is more important than the radiative charge-transfer process at the very low collision energies of 2×10^{-10} – 2×10^{-2} eV/u.

We also present the rate coefficients of nonradiative and radiative processes for the temperature range of 3×10^4 – 2×10^9 K and 10^{-6} – 10^3 K, respectively, which has important application in astrophysics and plasma physics.

ACKNOWLEDGMENTS

This work was supported by the National Basic Research program of China under Grant No. 2013CB922200 and the National Natural Science Foundation of China under Grants No. 11179041, No. 11474032, No. 11474033, and NSAF under Grant No. U1330117.

-
- [1] J. Weiner, V. S. Bagnato, S. Zilio, and P. S. Julienne, *Rev. Mod. Phys.* **71**, 1 (1999).
- [2] P. L. Gould, P. D. Lett, P. S. Julienne, W. D. Phillips, H. R. Thorsheim, and J. Weiner, *Phys. Rev. Lett.* **60**, 788 (1988).
- [3] R. Côté and A. Dalgarno, *Phys. Rev. A* **62**, 012709 (2000).
- [4] T. G. Lee, H. Nguyen, X. Flechard, B. D. DePaola, and C. D. Lin, *Phys. Rev. A* **66**, 042701 (2002).
- [5] M. van der Poel, C. V. Nielsen, M. Rybaltov, S. E. Nielsen, M. Machholm, and N. Andersen, *J. Phys. B: At. Mol. Opt. Phys.* **35**, 4491 (2002).
- [6] M. Lysebo and L. Veseth, *Phys. Rev. A* **77**, 032721 (2008).
- [7] L. L. Yan, L. Liu, Y. Wu, Y. Z. Qu, J. G. Wang, and R. J. Buenker, *Phys. Rev. A* **88**, 012709 (2013).
- [8] H. L. Daley and J. Perel, in *1969 Proceedings of the 6th International Conference on Physics of Electronic and Atomic Collisions* (MIT Press, Cambridge, MA, 1969), Abstracts, p. 1051.
- [9] R. E. Olson, *Phys. Rev. A* **2**, 121 (1970).
- [10] C. Bottcher and M. Oppenheimer, *J. Phys. B: At. Mol. Opt. Phys.* **5**, 492 (1972).
- [11] C. F. Melius and W. A. Goddard III, *Chem. Phys. Lett.* **15**, 524 (1972).
- [12] C. F. Melius and W. A. Goddard, III, *Phys. Rev. Lett.* **29**, 975 (1972).
- [13] R. E. Olson, *Phys. Rev. A* **6**, 1822 (1972).
- [14] D. Rapp and C.-M. Chang, *J. Chem. Phys.* **59**, 1276 (1973).
- [15] C. F. Melius and W. A. Goddard III, *Phys. Rev. A* **10**, 1541 (1974).
- [16] P. Habitz and W. H. E. Schwarz, *Chem. Phys. Lett.* **34**, 248 (1975).
- [17] T. R. Dinterman and J. B. Delos, *Phys. Rev. A* **15**, 463 (1977).
- [18] B. Hird and S. P. Ali, *Can. J. Phys.* **59**, 576 (1981).
- [19] R. J. Allan and J. Hanssen, *J. Phys. B: At. Mol. Opt. Phys.* **18**, 1981 (1985).
- [20] R. Shingal, C. J. Noble, B. H. Bransden, and D. R. Flower, *J. Phys. B: At. Mol. Opt. Phys.* **19**, 3951 (1986).
- [21] N. Vitanov and G. Panev, *J. Phys. B: At. Mol. Opt. Phys.* **25**, 239 (1992).
- [22] M. Machholm, E. Lewartowski, and C. Courbin, *J. Phys. B: At. Mol. Opt. Phys.* **27**, 4681 (1994).
- [23] R. J. Buenker and R. A. Phillips, *J. Mol. Struct.: THEOCHEM* **123**, 291 (1985).
- [24] S. Krebs and R. J. Buenker, *J. Chem. Phys.* **103**, 5613 (1995).
- [25] J. T. H. Dunning, *J. Chem. Phys.* **90**, 1007 (1989).
- [26] L. F. Pacios and P. A. Christiansen, *J. Chem. Phys.* **82**, 2664 (1985).
- [27] A. E. Kramida, Y. Ralchenko, J. Reader, and NIST ASD Team, NIST Atomic Spectra Database (ver. 5.0, online) (2012). Available at <http://physics.nist.gov/asd>.
- [28] B. Herrero, I. L. Cooper, and A. S. Dickinson, *J. Phys. B: At. Mol. Opt. Phys.* **29**, 5583 (1996).
- [29] G. Hirsch, P. J. Bruna, R. J. Buenker, and S. D. Peyerimhoff, *Chem. Phys.* **45**, 335 (1980).
- [30] M. Gargaud, R. McCarroll, and P. Valiron, *J. Phys. B: At. Mol. Opt. Phys.* **20**, 1555 (1987).
- [31] B. H. Bransden and M. R. C. McDowell, *Charge Exchange and the Theory of Ion-Atom Collisions* (Clarendon, Oxford, 1992).
- [32] M. C. Bacchus-Montabonel and P. Ceyzeriat, *Phys. Rev. A* **58**, 1162 (1998).
- [33] L. F. Errea, L. Mendez, and A. Riera, *J. Phys. B: At. Mol. Opt. Phys.* **15**, 101 (1982).

- [34] B. Zygelman, D. L. Cooper, M. J. Ford, A. Dalgarno, J. Gerratt, and M. Raimondi, *Phys. Rev. A* **46**, 3846 (1992).
- [35] W. Fritsch and C. D. Lin, *Phys. Rep.* **202**, 1 (1991).
- [36] B. R. Johnson, *J. Comput. Phys.* **13**, 445 (1973).
- [37] T. G. Heil, S. E. Butler, and A. Dalgarno, *Phys. Rev. A* **23**, 1100 (1981).
- [38] A. R. Turner, D. L. Cooper, J. G. Wang, and P. C. Stancil, *Phys. Rev. A* **68**, 012704 (2003).
- [39] B. Zygelman and A. Dalgarno, *Phys. Rev. A* **33**, 3853 (1986).
- [40] W. L. McMillan, *Phys. Rev. A* **4**, 69 (1971).
- [41] B. Zygelman and A. Dalgarno, *Phys. Rev. A* **38**, 1877 (1988).
- [42] P. C. Stancil and B. Zygelman, *Astrophys. J.* **472**, 102 (1996).
- [43] L. B. Zhao, P. C. Stancil, J. P. Gu, H.-P. Liebermann, Y. Li, P. Funke, R. J. Buenker, B. Zygelman, M. Kimura, and A. Dalgarno, *Astrophys. J.* **615**, 1063 (2004).
- [44] L. B. Zhao, J. G. Wang, P. C. Stancil, J. P. Gu, H. P. Liebermann, R. J. Buenker, and M. Kimura, *J. Phys. B: At. Mol. Opt. Phys.* **39**, 5151 (2006).
- [45] D. R. Bates, *Mon. Not. R. Astron. Soc.* **111**, 303 (1951).
- [46] M. Marinescu, H. R. Sadeghpour, and A. Dalgarno, *Phys. Rev. A* **49**, 982 (1994).
- [47] C. H. Liu, L. Liu, Y. Z. Qu, J. G. Wang, and R. K. Janev, *Phys. Rev. A* **82**, 022710 (2010).
- [48] C. H. Liu, Y. Z. Qu, J. G. Wang, Y. Li, and R. J. Buenker, *Phys. Rev. A* **81**, 012707 (2010).
- [49] X. J. Liu, Y. Z. Qu, B. J. Xiao, C. H. Liu, Y. Zhou, J. G. Wang, and R. J. Buenker, *Phys. Rev. A* **81**, 022717 (2010).
- [50] C. H. Liu, Y. Z. Qu, Y. Zhou, J. G. Wang, Y. Li, and R. J. Buenker, *Phys. Rev. A* **79**, 042706 (2009).
- [51] C. H. Liu, Y. Z. Qu, J. G. Wang, Y. Li, and R. J. Buenker, *Phys. Lett. A* **373**, 3761 (2009).
- [52] Z. Yu, Q. Yi-Zhi, L. Chun-Hua, and L. Xiao-Ju, *Chin. Phys. Lett.* **28**, 033401 (2011).